Materials Science Forum Vols. 143-147 (1994) pp 1311-1318
© (1994) Trans Tech Publications, Switzerland
doi:10.4028/www.scientific.net/MSF.143-147.1311
Materials Science Forum vols. 143-147 (1994) pp. 1311-1318
© Trans Tech Publications, Switzerland

SCANNING TUNNELING MICROSCOPY AND SPECTROSCOPY OF ARSENIC ANTISITE DEFECTS IN GaAs

R. M. FEENSTRA, J. M. WOODALL, AND G. D. PETTIT

IBM Research Division, T. J. Watson Research Center
Yorktown Heights, New York 10598 USA

Keywords: antisite, defect, tunneling, GaAs, EL2, STM, Coulomb gap

ABSTRACT

The scanning tunneling microscope (STM) is used to study thin layers of low-temperature-grown (LT) GaAs, containing about 1×10^{20} cm^{-3} arsenic-related defects. The studies are performed in cross-section, on the (110) cleavage edge of the LT-layers. Four types of defect images are observed, and are interpreted as arising from a single type of defect located at varying depths below the surface. Spectroscopy of the defect reveals an intense band of midgap states, which is identified with the EL2 level in GaAs. The defect is found to have full tetrahedral symmetry, with its core residing on the Ga-sublattice. Thus, the defect is identified as an isolated arsenic antisite (As on a Ga site), which is believed to be the dominant defect in LT-GaAs. Satellite features in the STM images are observed at distances of 15 Å away from the defect core, and are attributed to wave-function tails of the antisite defect. Observed gaps in the spectrum of midgap states are interpreted in terms of on-site and off-site Coulomb interactions (Hubbard U and Coulomb gap respectively).

1. INTRODUCTION

Over the past decade, the scanning tunneling microscope (STM) has been widely applied to the study of various types of surface specific defects (*e.g.* adsorbates, vacancies, structural disorder in surface reconstructions). However, application of the STM to the study of *bulk* defects has been much less common, with only a few such studies having been reported [1]. The focus on surface studies is understandable, since the STM specifically probes surface state-density (wave-function squared). Nevertheless, use of the STM to study defects which are distributed throughout a material (some of which happen to be located near a surface and thus are visible) can potentially yield new information on the structural and electronic properties of the defects.

In this paper, we report on STM studies of low-temperature-grown (LT) GaAs, which contains about 1×10^{20} cm^{-3} arsenic-related point defects [2]. With such a high concentration, it is relatively easy to locate, and study, individual defects. The LT-GaAs is grown as thin layers, on (001) oriented GaAs wafers. The STM work is then performed in a cross-sectional mode, in which the wafers are cleaved in ultra-high vacuum and the study is performed on the (110) cleavage face. This type of study (as opposed to studying the (001) growth surface) is advantageous since the (110) face is not reconstructed and the surface dangling bonds lie in energy outside of the bulk band gap [3–5]. Thus, studies of the (110) surface reveal properties, both geometric and electronic, which are similar to those found in the bulk.

On LT-GaAs layers, we observe in spectroscopy an intense band of midgap states, centered at about 0.5 eV above the valence-band maximum. This location of these states are close to those of a much studied defect in GaAs which produces the EL2 level, which is known to be the dominant defect in LT-GaAs [2,6]. This defect is known to involve an arsenic antisite (As on a Ga site), although considerable controversy surrounds the possibility of additional defects (such as an arsenic interstitial atom) also being involved [7–9]. We observe here that the defects are sym-

All rights reserved. No part of contents of this paper may be reproduced or transmitted in any form or by any means without the written permission of TTP, www.ttp.net. (ID: 169.237.79.123-04/02/13,22:07:42)

metric relative to the $(1\bar{1}0)$ mirror plane at the surface, thus indicating that they have full tetrahedral symmetry in the bulk. The position of the defect core is found to be on the Ga-sublattice. The derived structure is thus consistent with that of an isolated antisite defect. Detailed images of the antisite state-density are obtained, including satellite features which extend 15 Å away from the defect core. We argue that these satellites arise from tails of the antisite wave-function, possibly involving strain-related buckling effects on the surface [10]. The ability to resolve such detailed features in the defect wave-function indicates significant potential for the STM in structural determination for other types of defects as well.

2. EXPERIMENTAL

Our STM studies are performed in a cross-sectional mode, where a (001) GaAs wafer is cleaved in ultra-high-vacuum, and the STM probe-tip is stepped across the (110) cleavage face to the grown layers, at the edge of the cleavage face. This stepping process requires repeatable motion on the 1000 Å – 1 μm scale, which is obtained in our system by the use of piezoelectric "inchworms" [11]. A schematic of our STM design is given elsewhere [12]. With convenient computer control of the inchworms, it is possible to locate the grown layers in about 15 minutes. In order to obtain flat, high quality cleaves, thin substrates (100 μm thickness) are used. They are prepared by scribing a short notch using an *in situ* diamond scriber, and then pressing on the sample to break it at the cleave. Good cleaves are obtained on about 50% of the samples.

The LT-GaAs layers, typically 1000 Å thick, were grown in a Varian Gen-II MBE system at a growth temperature of 225°C. A cap layer grown at 350° C was grown on top of the LT-layer, and no subsequent annealing of the samples was performed. In addition to the 1×10^{20} cm^{-3} deep donor arsenic-related defects contained in the material, shallow donors or acceptors were also intentionally introduced. Three samples discussed here have shallow dopant concentrations of: n^+ (1×10^{19} cm^{-3} Si), p^+ (1×10^{19} cm^{-3} Be), and p^{++} (5×10^{19} cm^{-3} Be). The base pressure of the STM ultra-high-vacuum chamber is $< 4 \times 10^{-11}$ Torr. Single-crystal < 111 > oriented tungsten probe tips are used. Prior to use they are thoroughly cleaned by electron-bombardment heating, and characterized by field electron microscopy. Spectroscopic measurements were performed using a method previously developed for obtained a large dynamic range in the tunnel current and conductance [13]. Briefly, the tip-sample separation is varied as the voltage is scanned according to $\Delta s = -a \mid V \mid$, with $a \approx 1$ Å/V. Subsequent normalization is accomplished by computing the ratio of differential conductance dI/dV to total conductance $\overline{I/V}$, where the latter quantity is broadened over a range of 1.5 V [13]. Dynamic conductance is measured using a lock-in amplifier, with typically 50 mV modulation on the bias voltage. STM images are acquired with 0.1 nA constant-current, and at various voltages specified below.

3. RESULTS

In Fig. 1 we show STM images of the p^+ LT-GaAs layer. These images are acquired with negative sample bias, so that the background atomic corrugation arises from the As-sublattice of the GaAs. Numerous defects are visible in the images, and these defects can be classified into several types as labelled in Fig. 1. The largest apparent defect is type A, and the next largest is type B. Note the presence of two distinct satellite features on the left-hand side of the type B defects, and these satellites can be faintly seen around the type A defects as well. Other smaller types of defects are labelled C and D in Fig. 1, and most unlabeled defects in the images can be seen to fall within one of these four classes. As discussed in detail elsewhere [14], we interpret these various types of images as all arising from the same type of defect, with the core of the defect being located in differing planes relative to the (110) cleavage plane. Specifically, the image types A, B, C, and D are interpreted as arising from arsenic-related defects located 0, 1, 2, or 3 planes (2.0 Å spacing) below the surface.

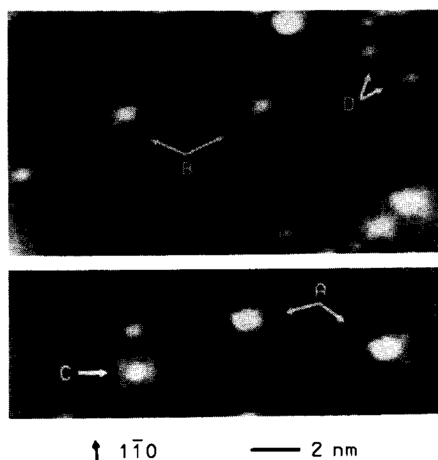

FIG. 1. STM images of the (110) cleaved surface of LT-GaAs, acquired at a sample voltage of − 2.0 V. Various point defects can be seen, and they are classified as types A, B, C, and D as indicated. The grey-scale range is 4.3 Å.

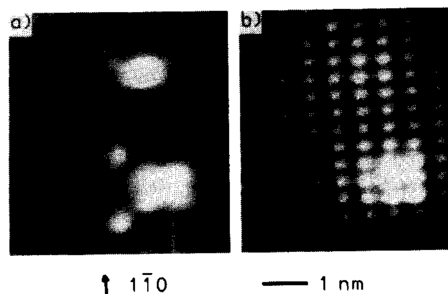

FIG. 2. STM image of identical surface regions, acquired at sample voltages of (a) − 2.0 and (b) +2.0 V. Defects of type B and C are seen.

Voltage-dependence of the STM images is shown in Fig. 2. We see that the empty state images, Fig. 2(b), show relatively little perturbation in the presence of the defects. The reason for this large voltage-dependence is the presence of filled states within the band gap, arising from the defects, as seen in the spectroscopy measurements below. For tunneling at negative voltages, the images include contributions from all filled states between the Fermi-levels of tip and sample, with the higher lying filled states (*i.e.* the defect states) contributing the most due to their higher tunneling probability. The tunnel current at positive voltages includes little or no contributions from the midgap defect states.

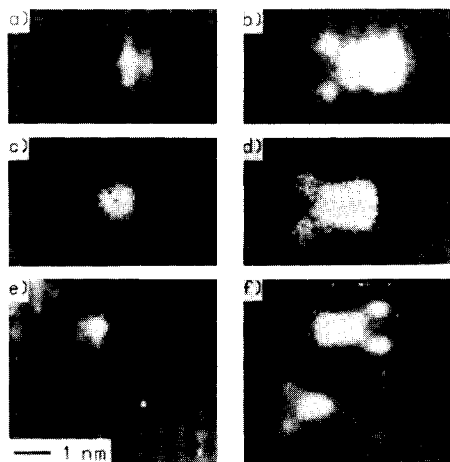

FIG. 3. Constant-current STM images (a), (c), and (e), and associated current images (b), (d), and (f) respectively. The images were acquired at sample voltages of (a) − 1.6, (b) − 0.5, (c) − 1.7, (d) − 1.0, (e) − 2.0, and (f) − 0.6 V. The current images include contributions only from the midgap defect states.

A direct method for obtaining images of the defect states within the band gap is to perform current imaging [15], that is, to acquire a constant-current image using some voltage outside the band gap, and then at each pixel to maintain a fixed tip-sample separation and measure the current at a voltage within the band gap region. Results for this type of measurement are shown in Fig. 3, with the measurements shown in the top (a and b), middle (c and d), and bottom (e and f) each obtained from different samples using different probe-tip geometries. The constant-current images (a, c, and e) appear different, depending on the sharpness of the probe-tip in the particular experiment. However, the current images (b, d, and f) all resemble each other. In particular, we observe the distinct satellite peaks around the defect images, with a type B defect seen in (b), (d) and the upper part of (f). We also note that the horizontal orientation of the satellite peaks in (f) is opposite that of (b) and (d) (*i.e.* the peaks are on the right-hand side of the defect core rather than the left). This difference occurs because sample (f) was cleaved along a $(1\bar{1}0)$ rather than a (110) plane, which produces a reversal in the sense of the [001] horizontal axis.

Spectroscopic results, obtained from the various samples specified in Section 2, are shown in Fig. 4. These results show typical spectra, averaged over about 10 defects for each sample. The spectra reveal tunneling out of valence-band states at large negative voltages and into conduction-band states at large positive voltages, with the band edges denoted by E_V and E_C respectively. These bands are separated by the bulk band gap of 1.43 eV. On a region of the LT-layer which is *not* on a point defect, the spectra reveal zero current and conductance within the gap. If the probe-tip is positioned on top of a point defect, then the spectra reveal large peaks within the gap region as seen in Fig. 4. Focussing first on Fig. 4(a), we find a band of states centered near $E_V + 0.5$ eV, and the Fermi-level (0 V) is located above this band. The location of this band is close to that for the donor states of an arsenic antisite defect [6], as shown in the top of Fig. 4 relative to the band edges of spectrum (a). Moving to Figs. 4(b) and (c), we see that as shallow acceptors are introduced into the material the Fermi-level moves into the band of deep defect states. Thus, these states are donors. For spectrum (c), in which the Fermi-level is roughly in the middle of the deep defect band, a distinct minimum in conductance forms at the Fermi-level, indicating a gap of about 0.4 eV in the state-density.

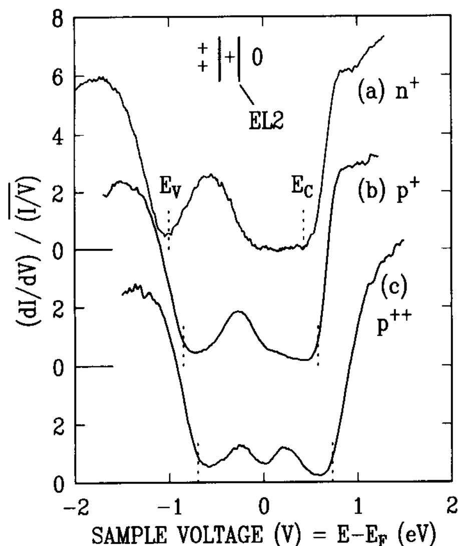

FIG. 4. Tunneling spectra acquired from layers of LT-GaAs containing varying amount of compensating shallow dopants. The valence-band maximum (E_V) and conduction-band minimum (E_C) are indicated by dashed lines in each spectrum. An intense band of states, arising from arsenic-related defects, appears within the band gap. The states of a bulk arsenic antisite defect are shown in the upper part of the figure, relative to the band edges of spectrum (a). The upper (0/+) state is the well-known EL2 level.

As discussed in the following section, the conductance minimum observed in Fig. 4(c) is interpreted in terms of Coulomb interactions at the defects. For the purpose of this interpretation it is useful to examine variation in spectra obtained over defects located at different spatial locations. The energy of the defect states vary at different locations due to the varying distance between the defect and neighboring defects and shallow dopants. This variation is shown in Fig. 5, for the p^+ sample, where we display individual spectra acquired at specific defect sites. Fig. 5(b) shows the most common result, appearing similar to Fig. 4(b). Figs. 5(a) and (c) are less commonly seen, and appear to have their average spectral weight shifted slightly up or down in energy (voltage) respectively compared to (b). Finally, Fig. 5(d) is the least common result, with the most low lying spectral weight. In terms of conductance minima, Figs. 5(a) and (b) display distinct minima at the Fermi-level (0 V), whereas Fig. 5(c) shows a weak minimum located at about – 0.3 V.

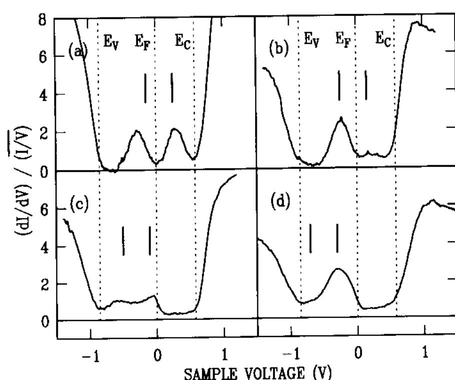

FIG 5. Tunneling spectra acquired from the p^+ LT-GaAs. Individual spectra are shown in (a)–(d), acquired from defects located a different spatial positions. The valence-band maximum (E_V), conduction-band minimum (E_C), and Fermi-level (E_F) are indicated by dashed lines in each spectrum. The spectra are interpreted in a two-level model, as shown by the heavy vertical lines in each panel.

4. DISCUSSION

The LT-GaAs studied here is know to contain about 1 atomic % excess arsenic atoms due to the low growth temperature [2]. In unannealed material, this excess arsenic gives rise to arsenic-related point defects, of which the dominant defect produces the well-known EL2 level in the material. That defect is known to involve as arsenic antisite (As on a Ga site), and it may involve other defects (such as arsenic interstitials) as well [7–9]. The concentration of the EL2-producing defects in LT-GaAs is typically $1 \times 10^{20}\,\mathrm{cm}^{-3}$. In our samples, the concentration of defects of the types seen in Fig. 1 is found to be in the range $(0.5 - 1) \times 10^{20}\,\mathrm{cm}^{-3}$. The agreement in these concentrations, together with the observation of midgap donor states at our defects, leads us to conclude that they are identical with the EL2-producing defects, thus being primarily composed of an arsenic antisite.

In terms of structure, the defects observed here all possess a single $(1\bar{1}0)$ mirror plane passing through the defect core (the antisite). This is the only symmetry present on the (110) surface. If the defects themselves have lower than tetrahedral symmetry, then, assuming they are randomly oriented relative to the surface, a fraction of the observed defects should violate this $(1\bar{1}0)$ mirror reflection. Even if the defects tended to orient themselves relative to the cleavage plane, we expect for defect complexes with low symmetry that the cleavage procedure will split some of the complexes (since they are certainly randomly oriented prior to cleaving), leading to a variation in the observed images and spectroscopy. Neither of these situations are seen here, and we conclude that the defects have tetrahedral symmetry, thus indicating that they consist of isolated antisite defects.

Satellite features are observed around the defects, seen most prominently for the type B images, with two satellite occurring at 15 Å from the defect core along $[1\bar{1}\bar{2}]$ and $[\bar{1}1\bar{2}]$ surface di-

rections. The possibility that the observed satellites arise from two (or more) additional defects (such as arsenic interstitials) can be excluded on the basis of spatially resolved spectroscopy measurements such as those shown in Fig. 3. Current images acquired at voltages throughout the band gap display a similar intensity ratio for the satellite features compared to the defect core, thus demonstrating that the spectrum of states measured over the satellites is basically the same as that acquired over the defect core. Thus, we conclude that the observed satellite features are purely electronic features of the defect, arising from tails of the antisite wave-function. The observed amplitude of the satellites corresponds to less than 1% of the state-density relative to that at the defect core. The satellite features probably arise from strain-related variations in surface buckling. Similar effects, though not so long-range, have been seen in recent computations for Si donors at the GaAs(110) surface [10].

We now turn to the spectroscopic results presented in Figs. 4 and 5. As seen in Fig. 4(a), an intense band of midgap donor states is observed, centered near $E_V + 0.5$ eV. The location of this band is close to the known donor levels associated with bulk antisite defects in GaAs as shown at the top of Fig. 4 (the upper level is the well-known EL2 level), and we thus identify our observed band with these levels. The width of the band we interpret as arising from Coulomb interactions between neighboring arsenic-related defects and with the shallow dopants: For a concentration of $N = 1 \times 10^{20}$ cm^{-3}, the average separation of defects is $N^{-1/3} = 22$ Å, leading to an energy scale for Coulomb interactions [16] of $e^2N^{1/3}/\varepsilon = 0.052$ eV for dielectric constant of $\varepsilon = 12.9$. The width of an impurity band due to Coulomb interactions is typically 5 times this value, or several tenths of an eV, which is consistent with that seen in Fig. 4 bearing in mind that there are two donor levels contributing to the observed spectral peak.

Coulomb interactions at the defect also are responsible for the observed conductance minimum, seen most clearly in Fig. 4(c). We can distinguish two types of effects: on-site Coulomb interactions, which lead to the Hubbard U splitting of the donor levels of the antisite defects (0.21 eV in the bulk [7]), and off-site Coulomb interactions which give rise to the Coulomb gap in an impurity band (this gap is typically twice the above Coulomb energy scale, or 0.1 eV [16]). The latter effect has significant consequences in the transport properties through impurity bands, giving rise to variable-range hopping and a temperature dependent activation energy for conduction. Such effects have indeed been reported for LT-GaAs [17], so the conduction mechanism through the defect states is well characterized (in contrast to most STM studies on semiconductor surfaces, where the conduction mechanisms are not well understood).

The above effects of Hubbard U splitting and Coulomb gap will both produce gaps in the observed spectrum of states. However, these gaps have differing behavior relative to the Fermi-level: the Coulomb gap is always centered about the Fermi-level, whereas the Hubbard U splitting is a property of the defect levels themselves and thus does not follow the Fermi-level. Thus, by studying the spectrum as a function of Fermi-level position, it should be possible to distinguish these effects of on-site and off-site Coulomb interaction. A hint of this behavior can already be seen in Fig. 4(b), where we find for the slightly empty donor band a weak inflection point at the Fermi-level, indicating a weak Coulomb gap. Clearer evidence is found in the individual spectra shown in Fig. 5. Those spectra were acquired over various defects, and the energy of the defect levels within the band gap will vary depending on proximity to neighboring defects. Thus, all of the spectra in Fig. 5 are interpreted in terms of a two-level system (using a splitting of 0.4 eV, to match the data), but the position of the levels varies relative to the Fermi-level. For Figs. 5(a) and (b), the Fermi-level is located between the two levels, and the conductance minimum occurs right at the Fermi-level. However, for the case of Fig. 5(c), both levels are seen to occur below the Fermi-level. A weak conductance minimum occurs near -0.3 V, which, being not at the Fermi-level, must arise from the Hubbard U gap. When the levels span the Fermi-level, as in Fig. 5(a) or Fig. 4(c), the observed gaps are much more pronounced, indicating that a Coulomb gap is making some contribution to the observed spectra. Finally, when both levels are well below the

Fermi-level, the spectrum has the appearance of a single large maximum, as shown in Fig. 5(d) or Fig. 4(a).

5. CONCLUSIONS

In summary, we have used the STM to observe properties of arsenic-related defects in LT-GaAs. We observe a characteristic defect, located on the Ga-sublattice, which satisfies the $(1\bar{1}0)$ mirror plane symmetry on the surface. This defect induces a band of donor states located near $E_V + 0.5$ eV which we identify with the well-known EL2 level (and associated second donor level) in GaAs, which is known to involve an arsenic antisite defect [7–9]. We thus identify our defect as being primarily composed of an arsenic antisite defect. Based on the observed symmetry and spectroscopic properties, we argue that this antisite is isolated (*i.e.* not involving a second structural defect) and in a tetrahedral environment, consist with that found in recent optical studies [9]. Long-range satellite features observed in the images are believed to arise from tails of the antisite wave-function. A more complete understanding of these features may lead to further structural information concerning this defect. For the high defect densities encountered in LT-GaAs, Coulomb interactions between neighboring defects gives rise to a distribution of impurity levels, with breadth of several tenths of an eV. Gaps are observed in the spectrum of this impurity band. Based on the behavior of these gaps as a function of Fermi-level position, it is demonstrated that they arise from a combination of on-site and off-site Coulomb interactions (Hubbard U and Coulomb gap respectively).

This study of LT-GaAs illustrates the strength of STM investigations of point defects, namely, the ability to observe both electronic and structural features of the defect (by performing spectroscopic and imaging measurements). One weakness of STM studies is the lack of any definite chemical identification; one must have some idea of what chemical species are present in the sample before any identification can be made. This drawback was overcome in the present work by studying material which was known to contain a very high density of arsenic-related defects [2]. Of course, it may not be possible to prepare such special materials in all cases.

Another favorable feature of the STM technique is the ability to resolve not only point defects, but larger defect complexes as well. For LT-GaAs, it is known that annealing the material after growth produces large (50 Å) precipitates of the excess arsenic. These precipitates have been observed by transmission electron microscopy [18], and their electrical properties have been measured with the STM [19]. For particular preparation methods, it is possible to obtain both point defect and precipitates in the same material, and the STM allows us to study both in a comparative manner.

Concerning the properties of the EL2-producing defect in GaAs, it has been argued on the basis of optically detected electron-nuclear double resonance (ODENDOR) measurements that this defect consists of an arsenic antisite paired with an arsenic interstitial [8]. We note that, although the identification with arsenic-related defects is direct in these measurements, the association of the observed defect with the EL2 level is not so direct. Of course, defect complexes in general can and do occur, and it would not be surprising if arsenic antisite defects in GaAs existed in both isolated form, and paired with an interstitial atom. We thus suggest that the defect studied here is different than that seen in the ODENDOR work, thereby accounting for the discrepancy in the derived structures [9].

REFERENCES

1. G. Cox, D. Szynka, U. Poppe, K. H. Graf, K. Urban, C. Kisielowski-Kemmerich, J. Krüger, and H. Alexander, Phys. Rev. Lett. ***64***, 2402 (1990); J. Vac. Sci. Technol. B ***9***, 726 (1991).
2. See, *e.g.*, M. Kaminska and E. R. Weber, Mat. Sci. Forum ***83-87***, 1033 (1992) and references therein.
3. H. W. M. Salemink, O. Albrektsen, and P. Koenraad, Phys. Rev. B***45***, 6946 (1992).

4. R. M. Feenstra, E. T. Yu, J. M. Woodall, P. D. Kirchner, C. L. Lin, and G. D. Pettit, Appl. Phys. Lett. ***61***, 795 (1992).
5. A. Vaterlaus, R. M. Feenstra, P. D. Kirchner, J. M. Woodall, and G. D. Pettit, J. Vac. Sci. Technol. B, Jul/Aug (1993), to be published.
6. E. R. Weber, H. Ennen, U. Kaufman, J. Windscheif, J. Schneider, and T. Wosinski, J. Appl. Phys. ***53***, 6140 (1982).
7. J. Dabrowski and M. Scheffler, Phys. Rev. B***40***, 10391 (1989).
8. B. K. Meyer, D. M. Hofmann, J. R. Niklas, and J.-M. Spaeth, Phys. Rev. B***36***, 1332 (1987).
9. M. K. Nissen, A. Villemaire, and M. L. W. Thewalt, Phys. Rev. Lett. ***67***, 112 (1991).
10. J. Wang, T. A. Arias, J. D. Joannopoulos, G. W. Turner, and O. L. Alerhand, Phys. Rev. B ***47***, 10326 (1993).
11. Burleigh Instruments Inc., Fishers, New York.
12. R. M. Feenstra, in *21st International Conference on the Physics of Semiconductors*, eds. Ping Jiang and Hou-Zhi Zheng (World Scientific, Singapore, 1992), p. 357.
13. P. Mårtensson and R. M. Feenstra, Phys. Rev. B***39***, 7744 (1988).
14. R. M. Feenstra, J. M. Woodall, and G. D. Pettit, submitted to Phys. Rev. Lett.
15. R. J. Hamers, R. M. Tromp, and J. E. Demuth, Phys. Rev. Lett. ***56***, 1972 (1986).
16. B. I. Shklovskii and A. L. Efros, *Electronic Properties of Doped Semiconductors* (Springer-Verlag, Berlin, 1984).
17. M. Kaminska and E. R. Weber, in *20th International Conference on the Physics of Semiconductors*, eds. E. M. Anastassakis and J. D. Joannopoulos, (World Scientific, Singapore, 1990), p. 473.
18. A. C. Warren, J. M. Woodall, J. L. Freeouf, D. Grischkowsky, D. T. McInturff, M. R. Melloch, and N. Otsuka, Appl. Phys. Lett. ***57***, 1331 (1990).
19. R. M. Feenstra, A. Vaterlaus, J. M. Woodall, and G. D. Pettit, submitted to Appl. Phys. Lett.

Defects in Semiconductors 17
10.4028/www.scientific.net/MSF.143-147

Scanning Tunneling Microscopy and Spectroscopy of Arsenic Antisite Defects in GaAs
10.4028/www.scientific.net/MSF.143-147.1311